J|A|C|S
ARTICLES
Published on Web 03/08/2007

Synthesis, Characterization, and Photoinduced Electron Transfer in Functionalized Single Wall Carbon Nanohorns

Carla Cioffi,[†] Stéphane Campidelli,*[,†] Chloé Sooambar,[†] Massimo Marcaccio,[‡] Gabriele Marcolongo,[§] Moreno Meneghetti,*[,§] Demis Paolucci,[‡] Francesco Paolucci,*[,‡] Christian Ehli,[||] G. M. Aminur Rahman,[||] Vito Sgobba,[||] Dirk M. Guldi,*[,||] and Maurizio Prato*[,†]

Contribution from the INSTM, Unit of Trieste, Dipartimento di Scienze Farmaceutiche, Università di Trieste, Piazzale Europa 1, I-34127 Trieste, Italy, INSTM, Unit of Bologna, Dipartimento di Chimica, Università di Bologna, Via Selmi 2, I-40126 Bologna, Italy, Dipartimento di Scienze Chimiche, Università di Padova, Via Marzolo 1, I-35131 Padova, Italy, and Institute of Physical Chemistry and Interdisciplinary Center for Molecular Materials (ICMM), Friedrich-Alexander-Universität Erlangen-Nürnberg, Egerlandstrasse 3, D-91058 Erlangen, Germany

Received November 9, 2006; E-mail: prato@units.it

Abstract: Single-wall carbon nanohorns (SWNHs) are a new class of material that is closely related to single-wall carbon nanotubes. Here, we describe the synthesis and characterization of a series of SWNHs functionalized with ethylene glycol chains and porphyrins. Functionalization of carbon nanohorns has been achieved using two different synthetic protocols: (1) direct attack of a free amino group on the nanohorn sidewalls (nucleophilic addition) and (2) amidation reaction of the carboxylic functions in oxidized nanohorns. The nanohorn derivatives have been characterized by a combination of several techniques, and the electronic properties of the porphyrin/nanohorn assemblies (SWNH/H_2P) have been investigated by electrochemistry, spectroelectrochemistry, and a series of steady-state and time-resolved spectroscopy. The cyclic voltammetry curve of nanohorn/porphyrin conjugate **6** showed a continuum of faradic and pseudocapacitive behavior, which is associated with multiple-electron transfers to and from the SWNHs. Superimposed on such a pseudocapacitive current, the curve also displays three discrete reduction peaks at −2.26, −2.57, and −2.84 V and an oxidation peak at 1.12 V (all attributed to the porphyrin moiety). Steady-state and time-resolved fluorescence demonstrated a quenching of the fluorescence of the porphyrin in SWNH/H_2P conjugates **5** and **6** compared to the reference free base porphyrin. Transient absorption spectra permitted the electron-transfer process between the porphyrins and the carbon nanostructures to be highlighted.

Introduction

Carbon-based nanomaterials are currently under active investigation for producing innovative materials, composites, and electronic devices of greatly reduced size.[1−5] Among the wide variety of carbon materials (which include fullerenes, single- and multiple-wall carbon nanotubes, carbon fibers, and carbon nanoonions),[6,7] single-wall carbon nanohorns (SWNHs) are of particular interest since these compounds possess high porosity and large surface areas. SWNHs are typically constituted by tubes of about 2−5 nm diameter and 30−50 nm length which associate to give rise to round-shaped aggregates of 100 nm diameter. Their surface areas and porosity ensure a great affinity for organic compounds[8−10] and make them promising candidates for hydrogen and methane storage[11−14] as well as for drug delivery systems.[15]

[†] Università di Trieste.
[‡] Università di Bologna.
[§] Università di Padova.
[||] Friedrich-Alexander-Universität Erlangen-Nürnberg.

(1) Dresselhaus, M. S.; Dresselhaus, G.; Avouris, P. *Carbon Nanotubes: Synthesis, Structure, Properties, and Applications*; Springer-Verlag: Berlin, 2001.
(2) Gogotsi, Y. *Carbon nanomaterials*; CRC Press: Boca Raton, FL, 2006.
(3) Dai, L. *Carbon Nanotechnology: Recent Developments in Chemistry, Physics, Materials Science and Device Applications*; Elsevier Science: New York, 2006.
(4) Meyyapan, M. *Carbon Nanotubes-Science and Applications*; CRC Press: Boca Raton, FL, 2005.
(5) O'Connell, M. J. *Carbon Nanotubes: Properties and Applications*; CRC Press: Boca Raton, FL, 2006.
(6) Inagaki, M.; Kaneko, K.; Nishizawa, T. *Carbon* **2004**, *42*, 1401.
(7) Oku, T.; Narita, I.; Nishiwaki, A.; Koi, N.; Suganuma, K.; Hatakeyama, R.; Hirita, T.; Tokoro, H.; Fujii, S. Formation, Atomic Structures and Properties of Carbon Nanocage Materials. *Carbon, The Future Material for Advanced Technology Applications*; Topics in Applied Physics; Springer-Verlag: Berlin, 2006; p 187.
(8) Adelene Nisha, J.; Yudasaka, M.; Bandow, S.; Kokai, F.; Takahashi, K.; Iijima, S. *Chem. Phys. Lett.* **2000**, *328*, 381.
(9) Fan, J.; Yudasaka, M.; Kasuya, Y.; Kasuya, D.; Iijima, S. *Chem. Phys. Lett.* **2004**, *397*, 5.
(10) Yuge, R.; Yudasaka, M.; Miyawaki, J.; Kubo, Y.; Ichihashi, T.; Imai, H.; Nakamura, E.; Isobe, H.; Yorimitsu, H.; Iijima, S. *J. Phys. Chem. B* **2005**, *109*, 17861.
(11) Murata, K.; Kaneko, K.; Kanoh, H.; Kasuya, D.; Takahashi, K.; Kokai, F.; Yudasaka, M.; Iijima, S. *J. Phys. Chem. B* **2002**, *106*, 11132.
(12) Tanaka, H.; Kanoh, H.; El-Merraoui, M.; Steele, W. A.; Yudasaka, M.; Iijima, S.; Kaneko, K. *J. Phys. Chem. B* **2004**, *108*, 17457.
(13) Bekyarova, E.; Murata, K.; Yudasaka, M.; Kasuya, D.; Iijima, S.; Tanaka, H.; Kahoh, H.; Kaneko, K. *J. Phys. Chem. B* **2003**, *107*, 4681.
(14) Murata, K.; Hashimoto, A.; Yudasaka, M.; Kasuya, D.; Kaneko, K.; Iijima, S. *Adv. Mater.* **2004**, *16*, 1520.

 10.1021/ja068007p CCC: $37.00

Scheme 1 [a]

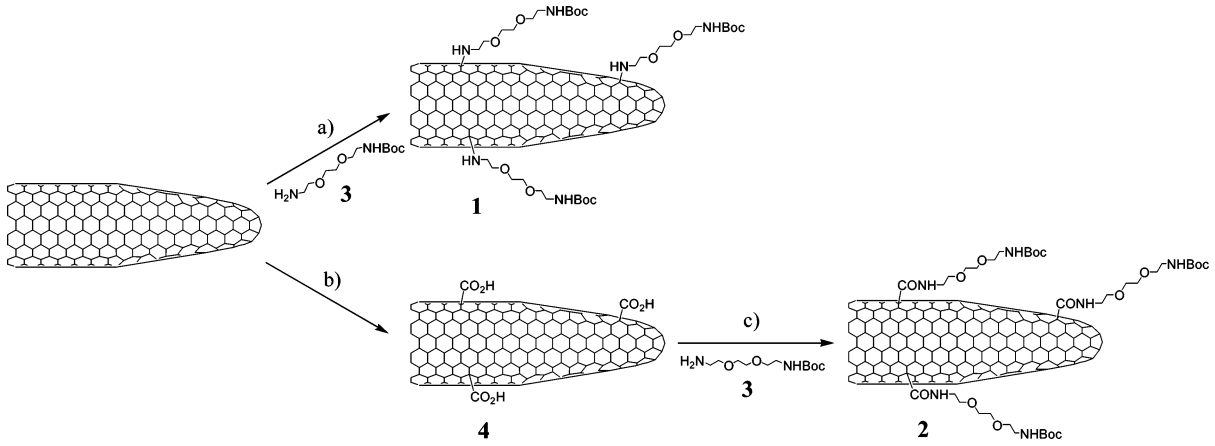

[a] Reagents and conditions: (a) DMF, 50 °C, 5 days; (b) piranha solution (H_2SO_4/H_2O_2, 30%, 4/1), rt, 3 h; (c) EDC, HOBt, DMF, 50 °C, 5 days.

Solubilization of nanohorns is a prerequisite for their applications in life science. Recently, several studies demonstrated that functionalization of SWNHs improved solubilization in organic solvents and in water.[16−18] Drug delivery systems based on functionalized nanohorns have generated great expectations.[15,19] Because SWNHs derive structurally from nanotubes, other applications can be envisaged for these compounds. Chemical derivatization with electroactive moieties can generate useful systems for electron-transfer and photovoltaic applications, similar to single-wall carbon nanotubes (SWNTs).[20−23]

Raman spectroscopy shows that SWNHs possess many more defects than SWNTs. For nanohorns, the disorder-induced D-band is similar in intensity to the graphite-like G-band.[16,24−26] This result is also corroborated by high-resolution transmission electron microscopy (HR-TEM) images in which it is possible to observe tortuous contours pointing outside of the central aggregates. The end caps and the presence of defects are known to introduce strain in the sp^2 framework of nanotubes, giving rise to areas with higher reactivity. In nanotubes, addition of an amine is possible at the cap region.[27] We expected similar or even higher reactivity for SWNHs, which we tested in reactions with amine derivatives. The presence of defects also facilitates the oxidation leading to formation of carboxylic groups, which are very versatile for subsequent functionalization.

Here, we describe the functionalization of pristine and oxidized SWNHs by direct nucleophilic addition or via amidation of the carboxyl groups, respectively, with a monoprotected diamine derivative as well as their subsequent derivatization with tetraphenylporphyrins. The electrochemical and photophysical properties of the SWNH/H_2P dyads have been investigated.

Results and Discussion

Synthesis and Characterization. The synthesis of the SWNH derivatives **1** and **2** is described in Scheme 1. The reaction of pristine SWNHs (p-SWNHs) in the presence of monoprotected diamine **3**[28] in DMF led to **1**. To produce **2**, p-SWNHs were first oxidized with piranha solution (H_2SO_4/H_2O_2 (30%), 4/1) to give nanohorns that bear carboxyl functionalities, **4** (ox-SWNHs), and then the latter were allowed to react with **3** in the presence of *N*-[3-(dimethylamino)propyl]-*N*′-ethylcarbodiimide (EDC) and 1-hydroxybenzotriazole (HOBt) in DMF to give **2**. The synthesis of dyads SWNH/H_2P **5** and ox-SWNH/H_2P **6** is described in Scheme 2. Nanohorns **1** and **2** were resuspended in DMF, and the *N*-*tert*-butoxycarbonyl (Boc) protecting group was removed by bubbling gaseous HCl through the suspension. The corresponding ammonium chloride salts precipitated during the acid treatment and were recovered by filtration over a Millipore membrane (Fluoropore, 0.22 μm). Finally the coupling between the ammonium salts derived from **1** and **2** and acid chloride **7** derived from 5,10,15-tris(3,5-di-*tert*-butylphenyl)-20-[4-(carbonyloxy)phenyl] porphyrin (**8**)[29,30] in the presence of Et_3N gave donor−acceptor nanoconjugates **5** and **6**, respectively. Acid chloride **7** was prepared by reacting **8** with oxalyl chloride at room temperature in dry CH_2Cl_2.

Oxidation and functionalization of SWNHs is a convenient methodology for producing functional nanohorns.[31] Here, we also demonstrate that amino derivatives can react directly with p-SWNHs to give functionalized materials. Compounds **1**, **2**, **4**, **5**, and **6** were fully characterized by standard analytical

(15) Murakami, H.; Ajima, K.; Miyawaki, J.; Yudasaka, M.; Iijima, S.; Shiba, K. *Mol. Pharm.* **2004**, *1*, 399.
(16) Cioffi, C.; Campidelli, S.; Brunetti, F. G.; Meneghetti, M.; Prato, M. *Chem. Commun.* **2006**, 2129.
(17) Tagmatarchis, N.; Maigné, A.; Yudasaka, M.; Iijima, S. *Small* **2006**, *2*, 490.
(18) Isobe, H.; Tanaka, T.; Maeda, R.; Noiri, E.; Solin, N.; Yudasaka, M.; Iijima, S.; Nakamura, E. *Angew. Chem., Int. Ed.* **2006**, *45*, 6676.
(19) Matsumura, S.; Yudasaka, M.; Iijima, S.; Shiba, K. Presented at the conference Nanotube 2006, Nagano, Japan, 2006; Poster C.049.
(20) Guldi, D. M.; Rahman, G. M. A.; Zerbetto, F.; Prato, M. *Acc. Chem. Res.* **2005**, *38*, 871.
(21) Sgobba, V.; Rahman, G. M. A.; Guldi, D. M.; Jux, N.; Campidelli, S.; Prato, M. *Adv. Mater.* **2006**, *18*, 2264.
(22) Ehli, C.; Rahman, G. M. A.; Jux, N.; Balbinot, D.; Guldi, D. M.; Paolucci, F.; Marcaccio, M.; Paolucci, D.; Melle-Franco, M.; Zerbetto, F.; Campidelli, S.; Prato, M. *J. Am. Chem. Soc.* **2006**, *128*, 11222.
(23) Campidelli, S.; Sooambar, C.; Lozano-Diz, E.; Ehli, C.; Guldi, D. M.; Prato, M. *J. Am. Chem. Soc.*, in press.
(24) Kasuya, D.; Yudasaka, M.; Takahashi, K.; Kokai, F.; Iijima, S. *J. Phys. Chem. B* **2002**, *106*, 4947.
(25) Yang, C.-M.; Kasuya, D.; Yudasaka, M.; Iijima, S.; Kaneko, K. *J. Phys. Chem. B* **2004**, *108*, 17775.
(26) Yang, C.-M.; Noguchi, H.; Murata, K.; Yudasaka, M.; Hashimoto, A.; Iijima, S.; Kaneko, K. *Adv. Mater.* **2005**, *17*, 866.
(27) Basiuk, E. V.; Monroy-Peláez, M.; Puente-Lee, I.; Basiuk, V. A. *Nano Lett.* **2004**, *4*, 863.
(28) Kordatos, K.; Da Ros, T.; Bosi, S.; Vázquez, E.; Bergamin, M.; Cusan, C.; Pellarini, F.; Tomberli, V.; Baiti, B.; Pantarotto, D.; Georgakilas, V.; Spalluto, G.; Prato, M. *J. Org. Chem.* **2001**, *66*, 4915.
(29) Tamiaki, H.; Suzuki, S.; Maruyama, K. *Bull. Chem. Soc. Jpn.* **1993**, *66*, 2633.
(30) Luo, C.; Guldi, D. M.; Imahori, H.; Tamaki, K.; Sakata, Y. *J. Am. Chem. Soc.* **2000**, *122*, 6535.
(31) Pagona, G.; Tagmatarchis, N.; Fan, J.; Yudasaka, M.; Iijima, S. *Chem. Mater.* **2006**, *18*, 3918.

Scheme 2 [a]

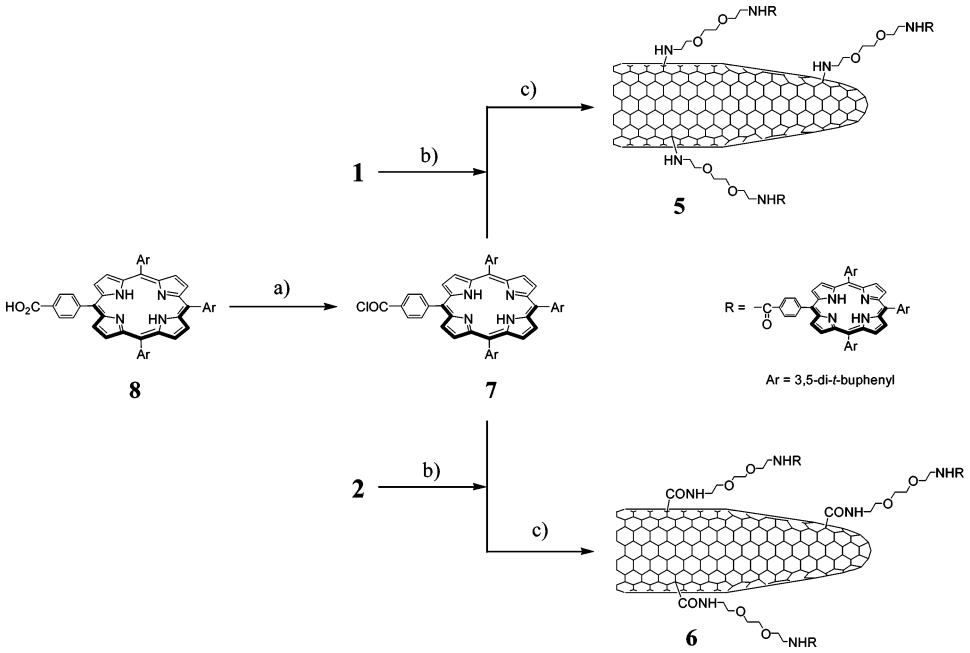

[a] Reagents and conditions: (a) oxalyl chloride, DMF(cat), CH_2Cl_2, rt, 20 h; (b) gaseous HCl, DMF, rt, 1 h; (c) Et_3N, DMF, CH_2Cl_2, rt, 4 days.

techniques, such as Raman, UV−vis, and FT-IR spectroscopies, thermogravimetric analysis (TGA), TEM, and atomic force microscopy (AFM).

FT-IR spectroscopy confirmed the presence of the carbonyl functions of the amide groups in **1**, **2**, **5**, and **6** (band around 1700 cm^{-1} corresponding to the stretching of the CO bond) and the presence of carboxyl groups for the ox-SWNHs **4** (band around 1750 cm^{-1}). Curiously, the bands around 2850−2950 cm^{-1} corresponding to the stretching of CH bonds are not visible in the spectra of the functionalized nanohorns **1** and **2**, while they are present in the spectra of the SWNH/H_2P derivatives **5** and **6** (see the Supporting Information).

The amount of organic groups in the functionalized SWNHs was determined by TGA. The thermograms of p-SWNHs, **1** and **2** are presented in Figure 1a,b. Nanohorn derivatives **1** and **2** present a loss of weight of about 16.5% and 30%, respectively, at 550 °C. This corresponds to one functional group per 105 and 55 carbon atoms of the nanohorn framework for **1** and **2**, respectively. It can be noticed that the loss of weight between 100 and 550 °C is constituted by two distinct events of similar intensity: first the loss of the Boc protecting group followed by degradation of the ethylene glycol chain. This result has also been observed in the case of a fullerene derivative bearing a similar chain used for comparison (Figure S1, Supporting Information).

TGA of **5**, **6**, and the porphyrin **8** are shown in Figure 1c,d. The porphyrin exhibits a characteristic thermogram with the first loss of weight before 300 °C, which may correspond to decarboxylation reaction, the second between 450 and 550 °C, and the third between 650 and 900 °C. The thermograms of the SWNH/H_2P conjugates **5** and **6** present some similarities to that of the porphyrin **8**, which confirms the presence of the porphyrin moiety. Compared to p-SWNHs, **5** and **6** give rise to a loss of weight of 47% and 53% at 900 °C, respectively. This corresponds to one functional group per 105 and 85 carbon atoms for **5** and **6**, respectively. We conclude that all the amino groups are linked to a porphyrin unit in nanoconjugate **5**, while a simple calculation permits a demonstration that **6** contains only one porphyrin for every two amino groups.

To be sure that for ox-SWNHs the attachment of amines does not take place by nucleophilic addition but really via the formation of amide bonds, we mixed the ox-SWNH derivative **2** with an excess of monoprotected diamine **3** under the same conditions as those for the synthesis of **1**. The resulting SWNHs were investigated by thermogravimetry. TGA did not show any significant changes before and after the reaction (Figure S2, Supporting Information). One possible explanation is that in ox-SWNHs all the defects to which the amine could react are oxidized, making the direct addition of amine to the carbon framework of the nanohorns impossible.

TEM−AFM. We investigated our SWNH derivatives by TEM. TEM images of all the compounds revealed the presence of nanohorns; in all cases the pictures consisted of small round-shaped aggregates with diameters of about 80−100 nm in which it was possible to distinguish small conical caps pointing out. Two representative images of SWNH **2** are shown in Figure 2 (additional pictures of **4** and **6** are shown in Figure S3, Supporting Information). Almost no difference can be noticed between the pristine material and the functionalized nanohorns.

Nanohorn derivatives **1**, **2**, **5**, and **6** have also been investigated by AFM. The samples were prepared by spin coating on a silicon wafer from a solution/suspension of the material in DMF. The images revealed in all cases the coexistence of individual SWNHs (round shapes of about 60−100 nm diameter) as well as aggregates several hundred nanometers high. Two representative images of SWNH/H_2P **6** are shown in Figure 3; the use of AFM did not allow us to see the fine structure of the nanohorns, and only some asperities on the surface have been observed.

Raman Spectra. Raman spectra of the p-SWNHs and of their derivatives—excitation at 633 and 488 nm—are reported in Figure 4. Raman spectra of SWNHs show two prominent bands

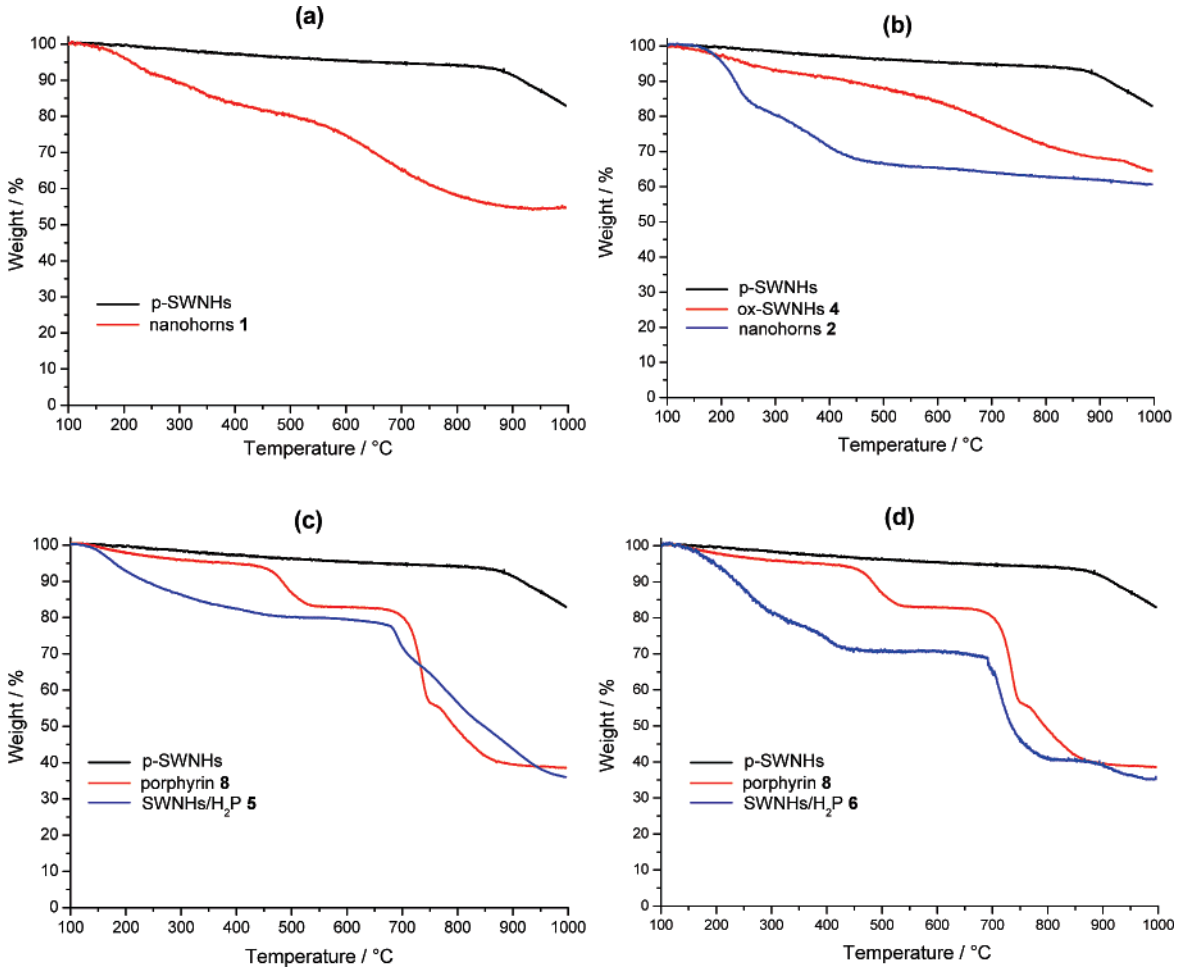

Figure 1. TGA curves recorded at 10 °C/min under N_2 of pristine and functionalized SWNHs: (a, b) SWNH derivatives containing protected ethylene glycol chains **1** and **2**; (c, d) SWNH/H_2P conjugates **5** and **6**.

at about 1350 (D-band) and 1590 (G-band) cm^{-1}. The D-band indicates, as usual for carbon nanostructures, the density of defects and can be used for monitoring the process of functionalization which transforms sp^2 to sp^3 sites. The spectra in Figure 4a,b, which are normalized with respect to the G-band, demonstrate that the oxidized nanotubes (i.e., **2** and **4**) show a larger number of defects than p-SWNHs and **1** since their D-band is more intense. It is also possible to note that the G-band of the functionalized compounds shows components at higher frequency in the spectra excited at 633 nm and some shifts at higher frequency when excitation is at 488 nm. Smaller shifts at higher frequency for the functionalized nanohorns can also be found for the D-band. This can be understood considering that the introduction of defects lowers the conjugation of the carbon network, which shifts the π electronic excitations to higher frequency. This is reflected in a higher frequency of the vibrational modes coupled to the π excitations. All these features show, therefore, that the functionalization was achieved.

Parts c and d of Figure 4 report the Raman spectra excited at 633 and 488 nm, respectively, of the dyads **5** and **6** and their comparison with the spectrum of the porphyrin and of the p-SWNHs. In both spectra the features related to the nanohorns and to the porphyrin are recognized. In Figure 4c the fluorescence of the porphyrin dominates the spectrum, but the bands of the SWNHs are easily seen. It is interesting to note that the broad band due to the fluorescence is found at smaller Raman shifts for **5** and **6** than for the original porphyrin. Moreover, also if we did not perform an absolute estimate of the intensity of the spectra, we found that, under similar conditions of excitation, the fluorescence of **5** and **6** was lower than what was found for the porphyrin. Both these characteristics of the spectra, the frequency shift and the intensity quenching, suggest that there is a clear interaction between SWNHs and porphyrin in dyads **5** and **6**.

In Figure 4d the fluorescence of the porphyrin is no longer present because we are recording the Raman signal in a spectral region where emission by the porphyrin is not present. In this case we observe a porphyrin band at 1555 cm^{-1} and another one, with smaller intensity, at 1499 cm^{-1}. The band at 1555 cm^{-1} can be easily recognized in the spectrum of **5** as a shoulder of the G-band of the nanohorn. In this case the D- and G-bands are not disturbed by the fluorescence, and they can be compared as in Figure 4b, confirming both the variation of the intensity of the D-band and the shift of the G-band at higher frequencies as a result of the functionalization.

Electrochemistry. The electrochemical behavior of SWNH/H_2P **6** was investigated in tetrahydrofuran (THF), with tetrabutylammonium hexafluorophosphate (TBAH) as the supporting electrolyte. The experiments were performed under ultradry conditions and at low temperature to have a wider potential window and to obtain a thorough characterization of the redox processes.

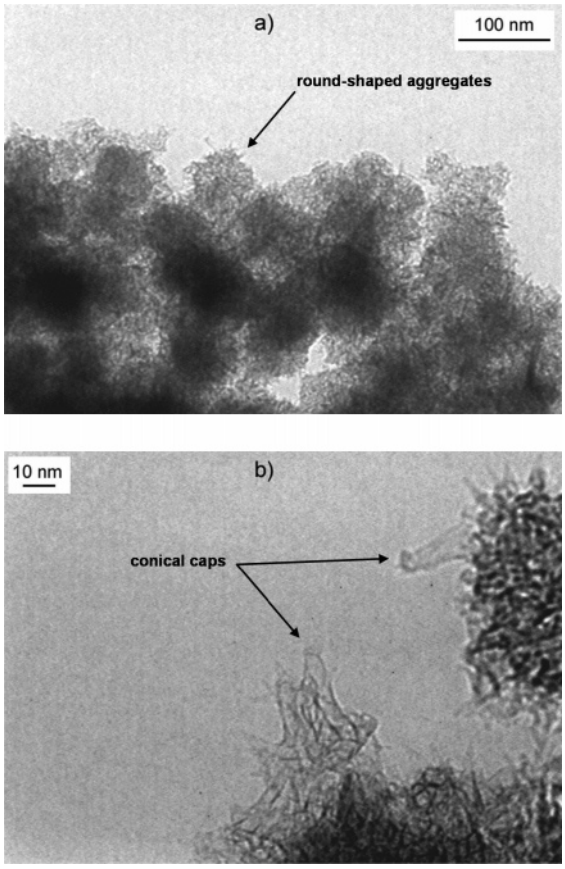

Figure 2. TEM images of the functionalized SWNH **2**: (a) low magnification, general view; (b) high magnification, close-up of the extremity of the aggregates showing end caps of the nanohorns.

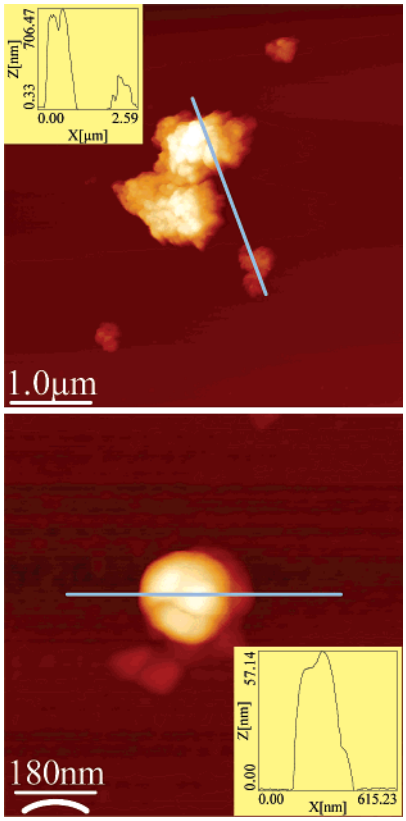

Figure 3. AFM images of SWNH/H_2P **6** prepared by spin coating on a silicon wafer from a DMF solution: top, several aggregates of nanohorns; bottom, an isolated round-shaped SWNH.

The cyclic voltammetry (CV) curve of a saturated SWNH/H_2P **6**, 0.015 M TBAH/THF solution, is shown in Figure 5. The curve displays a pseudocapacitive behavior characterized by a continuous increase in current with potential at either negative or positive potentials, with an onset located at ~−0.29 V (Figure 5, inset). By comparison with the CV behavior of functionalized SWNTs investigated under similar conditions[32] and as predicted by theory,[33] the continuum of the voltammetric current was attributed to either the progressive filling of the empty electronic states of the nanohorns (at $E \leq -0.5$ V) or the emptying of filled states (at $E \geq 0.3$ V). Notably, superimposed on such a pseudocapacitive current, the curve also displays three discrete reduction peaks, with peak potentials at −2.26, −2.57, and −2.84 V. Such processes were associated with one-electron transfers localized on the porphyrin moieties by comparison with the porphyrin model **9** (see Figures S4 and S5, Supporting Information). Interestingly, the first two reduction peaks are largely shifted toward more negative potentials with respect to model **9**, whereas the separation between the two processes is maintained (see Table 1). Such a shift has likely to be attributed to the strong electronic interaction between SWNHs and porphyrin in dyad **6**, as also evidenced by the Raman experiments. On the other hand, the anodic shoulder observed in the positive potential region (at 1.12 V) is close to the anodic peak observed in the model (Table 1), thus suggesting that the above interactions seem to be much less effective in the case of the oxidation process. The porphyrin-centered voltammetric peaks are largely broadened with respect to the model, possibly a joint effect of mass transport (i.e., smaller diffusion coefficient) and charge-transfer kinetics (i.e., hindering of electronic interaction with the electrode surface) deriving from association of porphyrins with the SWNH.[34]

Further insight into the electronic properties of nanoconjugate SWNH/H_2P **6** was obtained upon its spectroelectrochemical characterization. Upon application of potentials corresponding to the multiple reduction of SWNHs (i.e., $E \leq -0.25$ V; see the inset in Figure 5), two intense absorption bands developed gradually at 2795 and 2848 nm (Figure 6) along with a significant decrease of π plasmon absorption bands (Figure 6, inset). Interestingly, the transition energy of the above bands (~0.4 eV) is consistent with the band gap values theoretically predicted for pristine SWNHs.[33] Further reduction of the solution at more negative potentials brought about irreversible spectral changes, and the original spectra were not recovered even after bulk oxidation.

This behavior, along with the observation of the absorption features of pristine SWNHs and the decrease in the π plasmon absorption (indicative of a partial flocculation), might suggest that the reduction induces degradation of the nanoconjugate by removing the functionalization.

Photophysics. The UV−vis spectra of p-SWNHs reveal a set of two maxima at 226 and 276 nm. Yet slightly different

(32) Melle-Franco, M.; Marcaccio, M.; Paolucci, D.; Paolucci, F.; Georgakilas, V.; Guldi, D. M.; Prato, M.; Zerbetto, F. *J. Am. Chem. Soc.* **2004**, *126*, 1646.
(33) Berber, S.; Kwon, Y.-K.; Tománek, D. *Phys. Rev. B* **2000**, *62*, R2291.
(34) Guldi, D. M.; Menna, E.; Maggini, M.; Marcaccio, M.; Paolucci, D.; Paolucci, F.; Campidelli, S.; Prato, M.; Rahman, G. M. A.; Schergna, S. *Chem.—Eur. J.* **2006**, *12*, 3975.

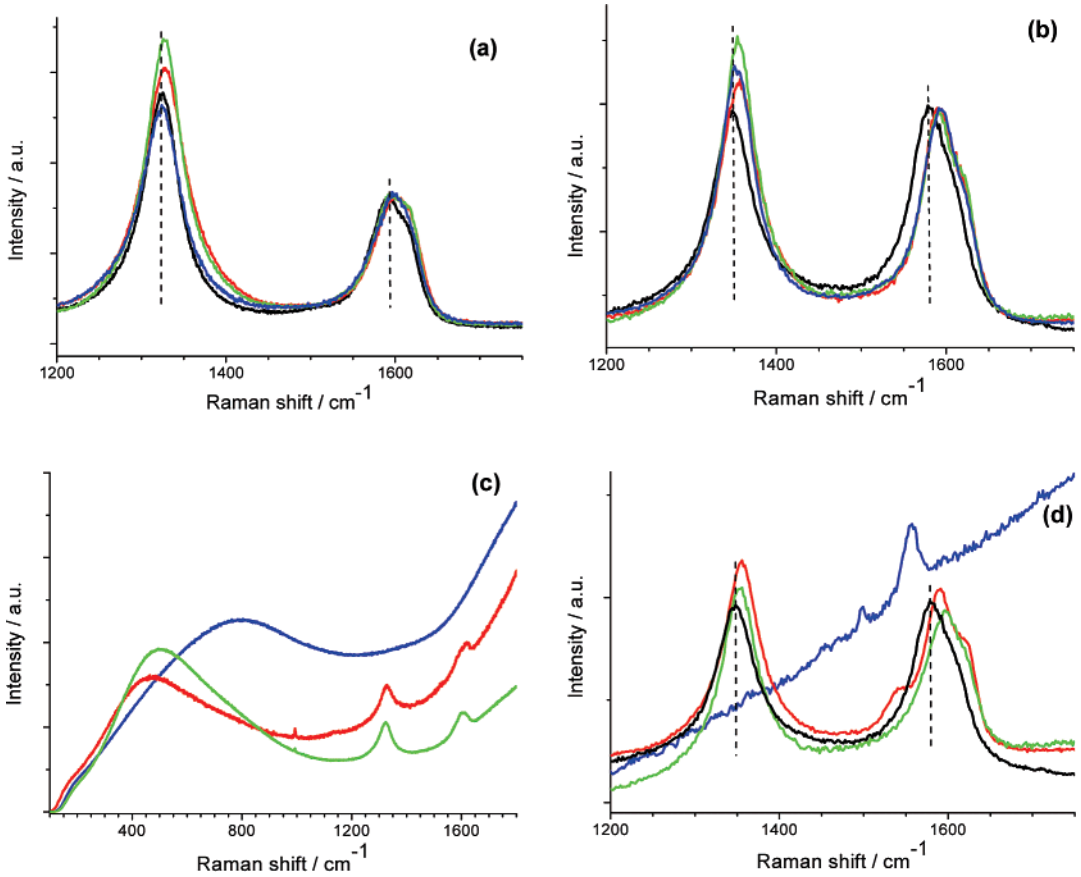

Figure 4. Raman spectra of pristine SWNHs and of the derivatives. Spectra in panels a and c are obtained with excitation at 633 nm and those in panels b and d with excitation at 488 nm. Key: (a, b) black line, p-SWNHs; red line, **4**; green line: **2**; blue line, **1**; (c, d) blue line, porphyrin **8**; green line, SWNH/H_2P **5**; red line, SWNH/H_2P **6**. The black line in panel d refers to pristine SWNHs.

are the spectra of functionalized SWNHs **1** and **2** and oxidized SWNH **4**. A broad absorption is noted for **1**, **2**, and **4** around 250 nm, which monotonically decreases in intensity until the near-infrared region (Figure S5). At first glance, the absorption spectra of SWNH/H_2P conjugates **5** and **6** provide unquestionable evidence for the presence of both constituents, namely, SWNHs and H_2P. In Figure 7, for example, the Soret band of H_2P is clearly discernible at 420 nm, while the Q-band features (i.e., 515, 550, 592, and 647 nm) are hardly visible. This effect is due to the strong π plasmon absorption bands of SWNHs—all throughout the visible part of the spectrum—that almost completely mask the H_2P transitions. However, a closer look reveals some notable differences between H_2P and SWNH/H_2P. First, a substantial broadening of the Soret band is apparent. Second, in SWNH/H_2P all features are red-shifted relative to the transitions seen in the H_2P reference (i.e., 417, 513, 548, 590, and 645 nm). We take these findings to postulate—in line with the electrochemical and Raman studies—the existence of electronic communications between the redox-active and photoactive components.

Further insight into electronic communications between the H_2P moieties and the SWNH core came from fluorescence measurements. In this respect, a reference solution of just H_2P (i.e., lacking SWNHs) in DMF was adjusted to match the absorption of SWNH/H_2P in DMF at the 420 nm excitation wavelength. Both samples (i.e., H_2P and SWNH/H_2P **6**) gave rise to the same fluorescence pattern; see Figure 8. In particular, sets of two fluorescence maxima—one around 650 nm and a second one around 715 nm—evolved. Besides a red shift (i.e., 653 and 718 nm) that qualitatively tracks the one observed in the ground-state absorption, an appreciable decrease in fluorescence intensity was seen for SWNH/H_2P. Setting both fluorescence spectra in relation, we derive a H_2P fluorescence quenching that is well in excess of 80%. For SWNH/H_2P **5** a similar trend evolved with a weaker H_2P fluorescence.

In time-resolved fluorescence measurements a monoexponential decay with a lifetime of 9.5 $\pm$ 0.5 ns was measured for the H_2P reference, when the 650 nm fluorescence maximum was analyzed. A complementary investigation with SWNH/H_2P **6** gave the best results (i.e., χ^2 of at least 1) when a biexponential fitting function with a long lifetime of 10.6 $\pm$ 0.5 ns and a short lifetime of 0.26 $\pm$ 0.5 ns with relative weight distributions of 77% and 23%, respectively, was applied. Notably, also in **5** a rapid fluorescence deactivation was recorded (i.e., 0.3 ns). The short lifetimes in both samples reflect electronic interactions and are assigned tentatively to a thermodynamically allowed electron-transfer process—vide infra. The starting point is the photoexcited singlet state of H_2P (1.9 eV) to yield either an oxidized SWNH/reduced H_2P (2.56 eV) or a reduced SWNH/oxidized H_2P (1.62 eV)—favoring, however, the latter process.

Next, we tested H_2P and SWNH/H_2P **6** in pump–probe experiments using 420 nm laser pulses from a Ti–sapphire laser. Figure 9 summarizes the results for the H_2P reference. Following the photoexcitation, a pattern developed that reflects largely the ground-state absorption: minima are discernible at 515, 550, 590, and 645 nm, and maxima are discernible at 470 and 690

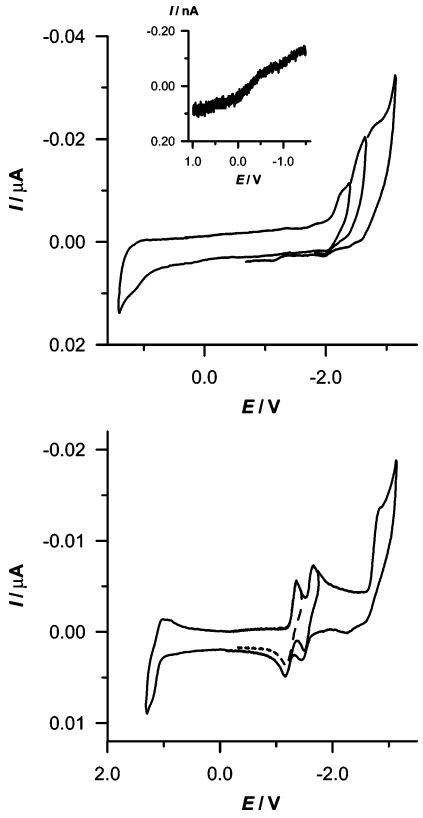

Figure 5. Top: CV curves in a 0.015 M TBAH/THF solution of saturated SWNH/H_2P **6** (inset, steady-state CV curve at 218 K), scan rate 0.5 V s^{-1} and Pt disk (10 μm diameter). Bottom: CV curves in a 0.4 mM solution of porphyrin model **9** in 0.015 M TBAH/THF. Data were recorded at 218 K and a scan rate of 1 V s^{-1}. The working electrode was a Pt disk (125 μm diameter). Potentials are referenced to SCE.

Table 1. Electrochemical Potentials (vs SCE)

Compound	$E_{1/2}$/V			
6[a]	1.10[c]	−2.23[c] (−2.11)	−2.58[c] (−2.43)	−2.82[c]
9[b]	1.19[c]	−1.27	−1.58	−2.81[c]

[a] Data collected for a solution of 0.4 mM, in 0.015 M TBAH/THF, at 1 V s^{-1} and 218 K. [b] Data collected for a saturated solution in 0.015 M TBAH/THF, at 1 V s^{-1} and 218 K. [c] E_p for quasi-reversible or totally irreversible behavior; in parentheses are given the $E_{1/2}$ values determined by digital simulation.

nm. These singlet excited-state features are stable on the time scale of our femtosecond experiments of 3.2 ns and only start to decay—through intersystem crossing to the triplet manifold—slowly.

In the corresponding SWNH/H_2P **6** experiments we note the following features at the end of the photoexcitation: minima at 520 and 555 nm and maxima at 480 and 700 nm. This confirms the successful excitation of the H_2P chromophores—to generate the H_2P singlet excited state—despite the dominating SWNH absorption. Again, even the excited-state features give rise to the red shift. In sharp contrast to the observation with the H_2P reference, the singlet excited state deactivated rapidly on our time scale. A lifetime of 0.1 ± 0.05 ns is derived from a multiwavelength analysis, for which an illustrative example is shown in Figure 10. Interestingly, the differential spectrum, as recorded at the end of the accelerated H_2P singlet excited state, is characterized by a broad feature (i.e., between 550 and 800 nm) that maximizes at around 625 nm. A plausible rationale for this observation implies an electron-transfer product that

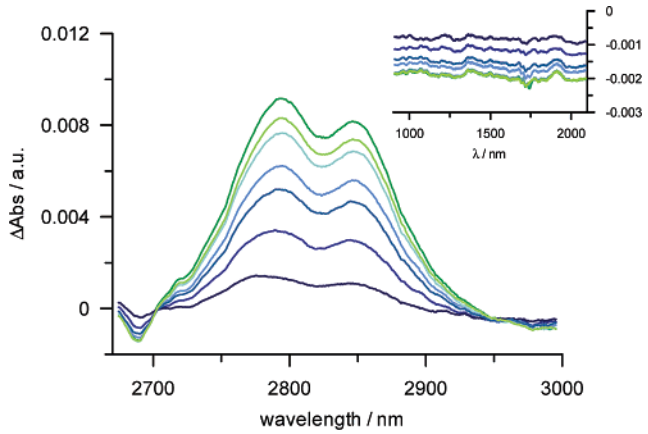

Figure 6. Difference absorption spectra recorded during reductive electrolysis of SWNH/H_2P **6**. The starting 0 mV applied potential was chosen as the reference. The potential was decreased from −300 mV (dark blue line) to −1800 mV (green line) by potential steps of 250 mV. Inset: detail of the π plasmon absorption region. Experimental conditions: 0.015 M TBAH, saturated THF solution, T = 298 K. Potentials are referenced to SCE.

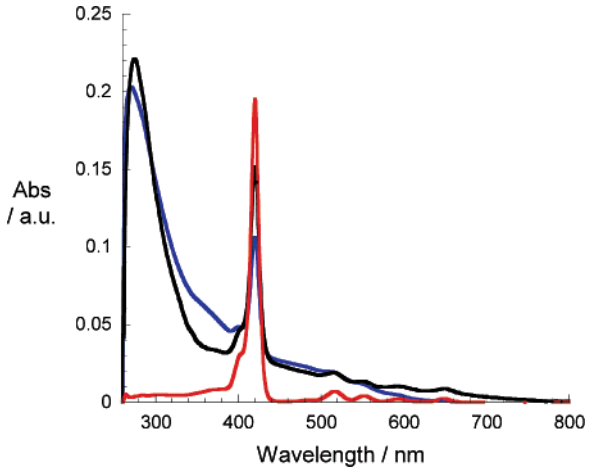

Figure 7. Absorption spectra of SWNT/H_2P **5** (blue line), SWNH/H_2P **6** (black line), and porphyrin **8** (red line) in DMF.

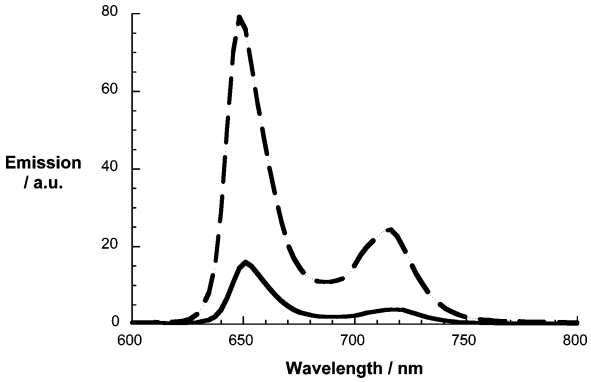

Figure 8. Steady-state fluorescence spectra of dilute DMF solutions of H_2P (dashed line) and SWNH/H_2P **6** (solid line) with matching absorption at the 420 nm excitation wavelength.

evolves from a photoinduced electron transfer between the photoexcited H_2P and SWNHs. This rationale is in line with the aforementioned evaluation (i.e., thermodynamic) of the electron-transfer pathways. Figure S6 (Supporting Information) demonstrates that in the case of photoexcited **5** at 420 nm the same electron-transfer product evolves.

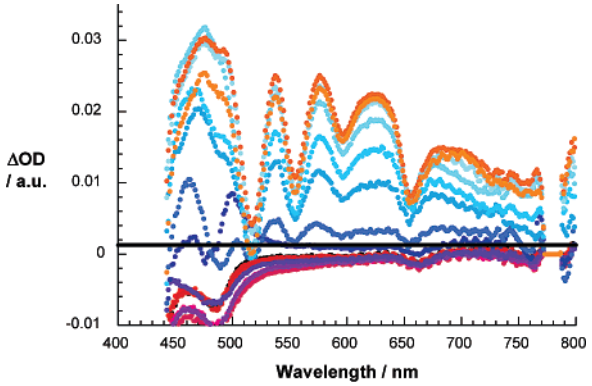

Figure 9. Differential absorption spectra (visible) obtained upon femtosecond flash photolysis (420 nm) of H_2P in nitrogen-saturated DMF solutions with several time delays between 0 and 5 ps at room temperature.

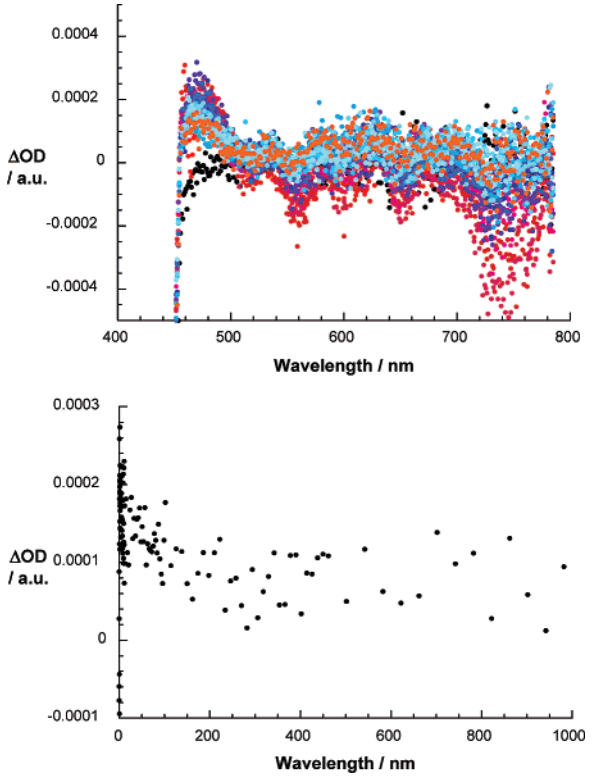

Figure 10. Top: differential absorption spectra (visible) obtained upon femtosecond flash photolysis (420 nm) of SWNH/H_2P **6** in nitrogen-saturated DMF solutions with several time delays between 0 and 300 ps at room temperature. Bottom: time−absorption profile of the spectra shown above at 465 nm.

Encouraged by our recent studies with SWNT—revealing characteristics for SWNT electron-transfer products in the near-infrared region—we recorded the differential absorption changes for SWNH/H_2P in a complementary experiment in the 800−1200 nm range. In fact, Figure 11 confirms nicely a strong bleaching of the SWNH absorptions in the near-infrared region. Important is the fact that the formation of this SWNH electron-transfer product develops concomitantly with the H_2P electron-transfer product in the visible region.

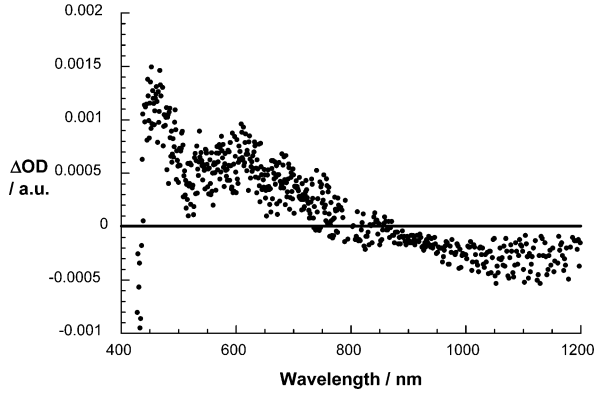

Figure 11. Differential absorption spectra (visible and near-infrared) obtained upon femtosecond flash photolysis (420 nm) of SWNH/H_2P **6** in nitrogen-saturated DMF solutions with a time delay of 300 ps at room temperature.

Conclusion

We described the functionalization of carbon nanohorns and the creation of new SWNH/porphyrin nanoconjugates. The functionalized SWNH derivatives have been characterized by a combination of techniques including thermogravimetry, FT-IR and Raman spectroscopy, and microscopy. All SWNHs exhibit reasonable solubility in organic solvents, and the properties of the SWNH/H_2P assemblies have been tested by means of electrochemical and photophysical measurements.

The CV curve of SWNH/H_2P **6** showed a continuum of faradic and pseudocapacitive behavior, which is associated with multiple-electron transfers to and from the SWNHs. Superimposed on such a current, the CV curve displayed also four discrete redox processes involving the porphyrin moiety. The electrochemical experiments revealed sizable electronic interactions of porphyrins with SWNHs in the aforementioned nanoconjugate. Furthermore, the spectroelectrochemistry exhibited the expected transition bands for pristine SWNHs, while it failed to produce the typical absorption peaks proper for porphyrin, likely because of chemical instability.

Steady-state and time-resolved fluorescence demonstrated a quenching of the fluorescence of the porphyrin in SWNH/H_2P conjugates **5** and **6** compared to the reference free base porphyrin. Transient absorption spectra permitted the electron-transfer process between the porphyrins and the carbon nanostructures to be highlighted.

Acknowledgment. This work was carried out with partial support from the University of Trieste, the University of Bologna, MIUR (PRIN, prot. 2006034372, 2004035502, and 2004035330 and Firb RBNE033KMA), EU (RTN network "WONDERFULL"), SFB 583, DFG (Grant GU 517/4-1), FCI, and the Office of Basic Energy Sciences of the U.S. Department of Energy (NDRL 4714).

Supporting Information Available: Technique and experimental details for the functionalization of nanohorns, additional thermogravimetric analyses, TEM pictures, and CV curve of the reference porphyrin **9**. This material is available free of charge via the Internet at http://pubs.acs.org.

JA068007P